Synthesis and Structural, Spectroscopic, and Magnetic Characterization of $(NH_4)[Fe_3(\mu_3\text{-}OH)(H_2L)_3(HL)_3]$ (H_3L = Orotic Acid) Presenting Two Novel Metal-Binding Modes of the Orotate Ligand: The Case of a Spin-Frustrated System

Catherine P. Raptopoulou,*,† Vaslis Tangoulis,*,‡ and Vassilis Psycharis

Institute of Materials Science, NCSR "Demokritos", 15310 Aghia Paraskevi, Athens, Greece

Received December 7, 1999

The use of orotic acid (H_3L) in iron(III) chemistry has yielded a structurally, magnetically, and spectrochemically very interesting complex. The 1:3:3 $FeCl_3 \cdot 6H_2O/H_3L$/aqueous NH_3 reaction system in MeOH gives red $(NH_4)[Fe_3(\mu_3\text{-}OH)(H_2L)_3(HL)_3] \cdot 7.75H_2O$ (**1**) in high yield. **1** crystallizes in the hexagonal space group $P\bar{3}$ with (at 25 °C) $a = 14.813(7)$ Å, $c = 15.084(7)$ Å, and $Z = 2$. There is a C_3 axis passing through the central hydroxo oxygen; thus, the three Fe^{III} atoms form an equilateral triangle with an edge of 3.312 Å and the $Fe_3O_{hydroxy}$ core is planar. The orotates present two novel coordination modes; each H_2L^- ligand bridges two Fe^{III} atoms through its *syn,syn* $\eta^1{:}\eta^1{:}\mu_2$ carboxylate group, while HL^{2-} simultaneously chelates one Fe^{III} atom through one carboxylate oxygen and the deprotonated amide nitrogen, and is bonded to a second metal ion through the adjacent carbonyl oxygen. The three H_2L^- and the three HL^{2-} ligands lie above and below the $Fe_3O_{hydroxy}$ plane, respectively. Hydrogen bonds between the orotates result in a 3D network. Magnetic measurements of **1** in the 1.8−300 K temperature range were fitted using a 2*J* model with mean-field corrections and show antiferromagnetic interactions between the metal ions in the trinuclear moiety as well as between the trimers due to the 3D H-bonded network. The case of spin frustration is discussed extensively as well as the possible antisymmetric exchange interactions. The solid state X-band EPR spectrum of **1** at 4 K is consistent with the magnetic measurements showing that the $S = {}^1/_2$ ground state is very close to the first excited $S = {}^3/_2$, which is also populated at this temperature. Furthermore, the simulation of the EPR spectrum reveals the anisotropic character of the system.

Introduction

The coordination chemistry of orotic acid (2,6-dioxo-1,2,3,6-tetrahydropyrimidine-4-carboxylic acid, vitamin B_{13}, H_3L, Chart 1) has been studied in detail in recent years, research in this area ranging from bioinorganic to pharmaceutical and materials chemistry. Attachment of a ribose phosphate group to orotate, assisted by metal ions and followed by decarboxylation, finally results in the formation of uridylate (UMP), one of the basic pyrimidine nucleotides synthesized in living organisms.[1] Moreover, metal ion orotates have been widely used in medicine; for example, platinum, palladium, and nickel orotate complexes have been screened as anticancer agents.[2,3] A biological carrier function has also been proposed for orotates resulting in using them to cure syndromes associated with the deficiency of metal ions, such as calcium, magnesium, zinc, or iron, in living organisms.[4−7]

Besides its important biological role, the mono- and dianion of orotic acid (H_2L^- and HL^{2-}) are potentially polydentate ligands. The crystallographically established coordination modes of H_2L^- and HL^{2-} are summarized in Chart 1. The monoanionic form of orotic acid behaves as a monodentate $O_{carboxylate}$ ligand (**I**) in tris(aqua)bis(orotato)dioxouranium(VI),[8] as an $O_{carboxylate}$, O(2) bidentate bridging ligand (**II**) in orotatobis(triphenylposphine)copper(II),[9] and as an $O_{carboxylate}$, O(2), O(4) μ_3 ligand (**III**) in aqua(orotato)lithium(I).[6] There have been two cases where H_2L^- does not participate in the coordination sphere of magnesium(II)[6] and zinc(II),[5] but it is used to counterbalance the $[M(H_2O)_6]^{2+}$ cation. The HL^{2-} ligand is mainly coordinated via the deprotonated nitrogen N(1) and one of the carboxylate oxygens (**IV**) acting as a chelating agent,[5,10−14] but the mixed chelating−bridging modes **V**,[15] **VI**,[7,16] and **VII**[11] have also been observed. Recently,[17] Darensbourg et al. examined the binding

* Authors to whom correspondence should be addressed.
† Tel: +301-6503365. Fax: +301-6519430. E-mail: craptop@ims.demokritos.gr.
‡ Tel: +301-6503365. Fax: +301-6519430. E-mail: tangoulis@ims.demokritos.gr.

(1) Stryer, L. *Biochemistry*, 3rd ed.; W. H. Freeman and Company: New York, 1988; Chapter 25.
(2) Schidbaur, H.; Classen, H.-G.; Helbig, J. *Angew. Chem., Int. Ed. Engl.* **1990**, *29*, 1090.
(3) Solin, T.; Matsumoto, K.; Fuwa, K. *Bull. Chem. Soc. Jpn.* **1981**, *54*, 3731.
(4) Matsumoto, K. *Inorg. Chim. Acta* **1988**, *151*, 9.
(5) Kumberger, O.; Riede, J.; Schmidbaur, H. *Z. Naturforsch. B* **1993**, *48*, 961.
(6) Bach, I.; Kumberger, O.; Schmidbaur, H. *Chem. Ber.* **1990**, *123*, 2267.
(7) Kumberger, O.; Riede, J.; Schmidbaur, H. *Chem. Ber.* **1991**, *124*, 2739.
(8) Mentzafos, D.; Katsaros, N.; Terzis, A. *Acta Crystallogr.* **1987**, **C***43*, 1905.
(9) Darensbourg, D. J.; Larkins, D. L.; Reibenspies, J. H. *Inorg. Chem.* **1998**, *37*, 6125.
(10) (a) Sabat, M.; Zlinska, D.; Jezowska-Trzebiatowska, B. *Acta Crystallogr.* **1980**, *B36*, 1187. (b) Mutikainen, I.; Lumme, P. *Acta Crystallogr.* **1980**, *B36*, 2233. (c) Kubiac, M.; Thomas, B. *Acta Crystallogr.* **1986**, *C42*, 1705. (d) Mutikainen, I. *Inorg. Chim. Acta* **1987**, *136*, 155.
(11) Nepveu, F.; Gaultier, N.; Korber, N.; Jaud, J.; Costan, P. *J. Chem. Soc., Dalton Trans.* **1995**, 4005.
(12) Burrows, A. D.; Mingos, D. M. P.; White, A. J. P.; Williams, D. J. *J. Chem. Soc., Dalton Trans.* **1996**, 149.
(13) Mutikainen, I.; Hämäläinen, R.; Klinga, M.; Orama, O.; Turpeinen, U. *Acta Crystallogr.* **1996**, *C52*, 2480.
(14) James, S. L.; Mingos, D. M. P.; Xu, X.; White, A. J. P.; Williams, D. J. *J. Chem. Soc., Dalton Trans.* **1998**, 1335.

10.1021/ic9914084 CCC: $19.00
Published on Web 09/09/2000

Chart 1

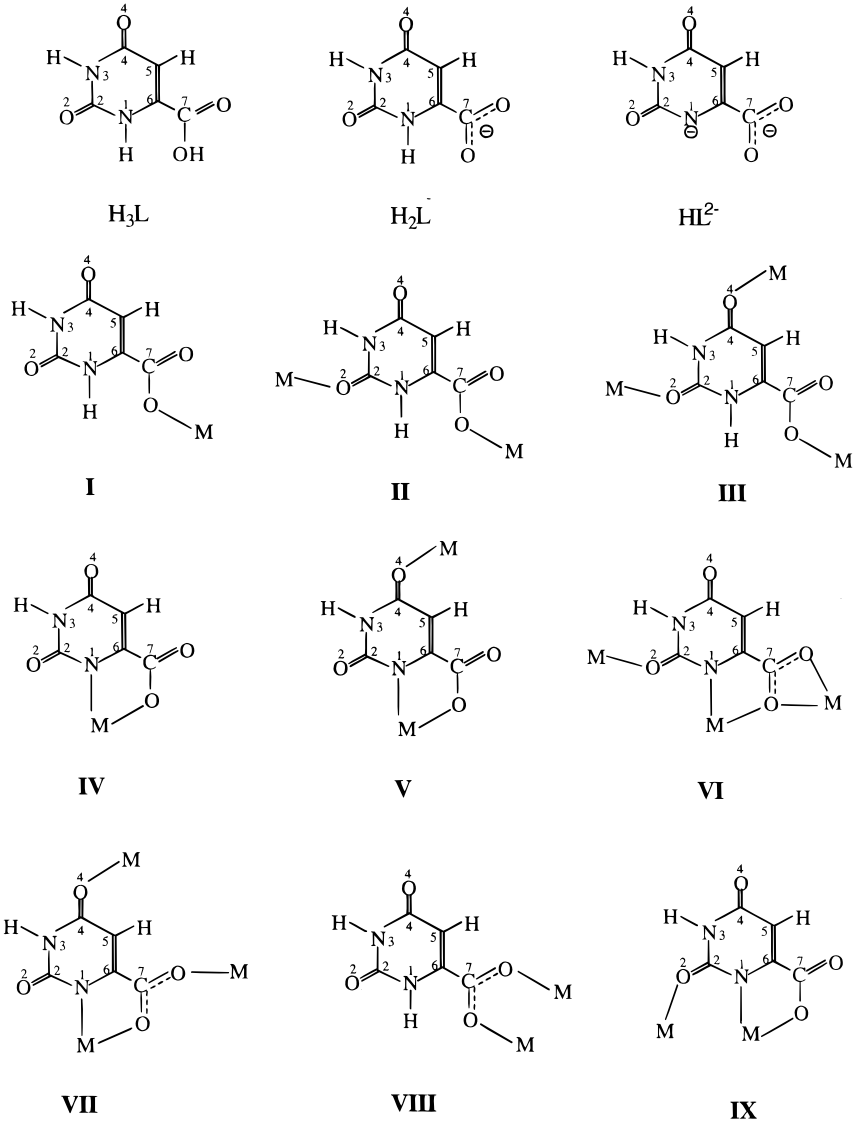

of HL^{2-} in organometallic derivatives, namely, group 6 metal carbonyls. These studies demonstrated that the coordination mode of the ligand is **IV** and that the chelated, deprotonated nitrogen of the uracil ring can exhibit significant π-donating capability and thus greatly enhance CO lability in these metal carbonyl complexes.

No matter how the orotate is coordinated to metal ions, it still has available donor and acceptor atoms capable of participating in hydrogen bonds. This property establishes orotate as a significant candidate for designing supramolecular structures based on its metal ion complexes.[11,13,18] Supramolecular aggregates of this type play an important role in metallodrug design as well as in materials chemistry.[19] The incorporation of metals into supramolecular systems succeeds in transferring magnetic and optical properties of the metal ions into these systems.

Our interest in the chemistry of binuclear and polynuclear iron complexes with O, N donor ligands comes from their biological importance[20] as well as their interesting magnetic behavior. Trinuclear oxo-centered iron complexes, of the general formula $[Fe_3(\mu_3\text{-}O)(O_2CR)_6L_3]^{z+}$ ($z = +1$, 0 and L = neutral monodentate ligand), known as "basic carboxylates", have been studied intensively for over 50 years.[21] The Fe_3O group is planar, or nearly so, and equilateral, or nearly so, but slight deviations from trigonal symmetry are found in many cases and can be of considerable interest in affecting their physical properties. These systems combine high symmetry and large nonbonding metal−

(15) (a) Khodashova, T. S.; Porai-Koshits, M. A.; Dacidenco, N. K.; Vlasova, N. N. *Sov. J. Coord. Chem.* **1984**, *10*, 141. (b) Mutikainen, I. *Finn. Chem. Lett.* **1985**, 193.
(16) Mutikainen, I. *Recl. Trav. Chim. Pays-Bas* **1987**, *106*, 438.
(17) Darensbourg, D. J.; Draper, J. D.; Larkins, D. J.; Frost, B. J.; Reibenspies, J. H. *Inorg. Chem.* **1998**, *37*, 2538.
(18) Burrows, A. D.; Mingos, D. M. P.; White, A. J. P.; Williams, D. J. *J. Chem. Soc., Dalton Trans.* **1996**, 3805.
(19) (a) Lehn, J.-M. *Angew. Chem., Int. Ed. Engl.* **1988**, *27*, 89. (b) Burrows, A. D.; Chan, C.-W.; Chowdhry, M. M.; McGrady, J. E.; Mingos, D. M. P. *Chem. Soc. Rev.* **1995**, 329.
(20) (a) Lippard, S. J. *Angew. Chem., Int. Ed. Engl.* **1988**, *27*, 344. (b) Kurtz, D. M., Jr. *J. Biol. Inorg. Chem.* **1997**, *2*, 159.
(21) (a) Cannon, R. D.; White, R. P. *Prog. Inorg. Chem.* **1988**, *36*, 195. (b) Degang, F.; Guoxiong, W.; Wenxia, T.; Kaibei, Y. *Polyhedron* **1993**, *20*, 2459. (c) Holt, E. M.; Holt, S. L.; Tucker, W. F.; Asplund, R. O.; Watson, K. J. *J. Am. Chem. Soc.* **1974**, *96*, 2621. (d) Lynch, V. M.; Sibert, J. W.; Sessler, J. L.; Davis, B. E. *Acta Crystallogr.* **1991**, *C47*, 866. (e) Blake, A. B.; Fraser, L. R. *J. Chem. Soc., Dalton Trans.* **1975**, 193. (f) Gorun, S. M.; Lippard, S. J. *J. Am. Chem. Soc.* **1985**, *107*, 4568. (g) Thundathil, R. V.; Holt, E. M.; Holt, S. L.; Watson, K. J. *J. Am. Chem. Soc.* **1977**, *99*, 1818. (h) Giacovazzo, C.; Scordari, F.; Menchetti, S. *Acta Crystallogr.* **1975**, *B31*, 2171. (i) Anzenhofer, K.; De Boer, J. J. *Recl. Trav. Chim.* **1969**, *88*, 286.

metal distances and have been used as fundamentals for the understanding of magnetic and electronic interactions. For Fe(III) "basic carboxylates" typical J values resulting from the equilateral-triangle model are $\sim$60 cm^{-1}, and as a result their highest spin states are not significantly populated at room temperature. Moreover, the energy gap between the ground state and the first excited multiplet can be as large as 50 cm^{-1} and therefore the ground state is almost "isolated". The monocationic species were the first polynuclear systems used to understand the magnetic interactions in exchange-coupled systems, while the neutral ones display temperature dependent mixed-valence behavior.[22] In the case of triiron(III) oxo-bridged complexes, it is firmly established that the metal ions are antiferromagnetically coupled, but all recent measurements indicate that the three magnetic coupling constants are not equal due to differences in metal−metal distances, metal−oxygen distances, or bond angles.[23]

The structural motif of the "basic carboxylates" is broken in cases where polydentate ligands have been used instead of the various carboxylates and/or the monodentate ones (L). Thus, mixed-valence trinuclear complexes[24] where all the RCO_2^- or all the neutral monodentate ligands have been substituted by polydentate L have been reported.

Herein we report the synthesis, crystal structure, and magnetic, EPR, and Mössbauer properties of the trinuclear complex $(NH_4)[Fe_3(\mu_3\text{-}OH)(H_2L)_3(HL)_3]\cdot 7.75H_2O$ (**1**), which is the first structurally characterized and studied orotato iron(III) complex exhibiting the new metal-binding modes **VIII** and **IX** for H_2L^- and HL^{2-}, respectively.

Experimental Section

Materials. All manipulations were performed under aerobic conditions using materials as received (Aldrich Co). All chemicals and solvents were of reagent grade.

Physical Measurements. Elemental analysis for carbon, hydrogen, and nitrogen was performed on a Perkin-Elmer 2400/II automatic analyzer. Infrared spectra were recorded as KBr pellets in the range 4000−500 cm^{-1} on a Bruker Equinox 55/S FT-IR spectrophotometer. Solid state EPR spectra were recorded on a Bruker ER 200D-SRC X-band spectrometer equipped with an Oxford ESR 9 cryostat in the 300−4 K temperature range. Variable temperature magnetic susceptibility measurements were carried out on a polycrystalline sample of **1** in the 300−1.8 K temperature range using a Quantum Design Squid susceptometer by applying a magnetic field of 6000 G. Magnetization measurements were carried out at the temperature range 1.8−4 K in the 0−5 T magnetic field range. The correction for the diamagnetism of the complex was estimated using Pascal's constants. Mössbauer spectra were taken with a constant acceleration spectrometer using a 60 mCi Co^{57} (Rh) source moving at room temperature and a variable temperature cryostat.

Preparation of $(NH_4)[Fe_3(\mu_3\text{-}OH)(H_2L)_3(HL)_3]\cdot 7.75H_2O$ (1). H_3L (0.468 g, 3.0 mmols) was added to warm MeOH and stirred under reflux for 10 min when an equimolar quantity of concentrated aqueous NH_3 was added. Orotic acid is insoluble in MeOH, but in the form of its ammonium salt it is slightly dissolved after stirring of the solution for another 10 min. $FeCl_3\cdot 6H_2O$ (0.270 g, 1.0 mmol) was then added, and an orange suspension was obtained. By continuing the reflux for another 60 min the reaction mixture gradually turned to red. The excess of orotic acid was then filtered, and the red filtrate was allowed to evaporate slowly. Red crystals of **1** were formed after 10 days (0.30 g, $\sim$71%), along with negligible amounts of an orange powder, which was removed by washing with MeOH. Anal. Calcd (found) for $C_{30}H_{35.5}N_{13}O_{32.75}Fe_3$: C, 28.38 (30.22); H, 2.82 (2.66); N, 14.34 (14.38).

Table 1. Crystallographic Data for Complex **1**·7.75H_2O

formula	$C_{30}H_{35.5}N_{13}O_{32.75}Fe_3$
fw	1269.71
space group	$P\bar{3}$ (No. 147)
T, °C	25
λ, Å	Mo Kα (0.71073 Å)
a, Å	14.813(7)
c, Å	15.084(7)
V, Å^3	2867(2)
Z	2
$\rho_{calcd}/\rho_{measd}$, g cm^{-3}	1.471/1.45
μ(Mo Kα), mm^{-1}	0.848
R1[a]	0.0621
wR2[a]	0.1755

[a] $w = 1/[\sigma^2(F_o^2) + (aP)^2 + bP]$ and $P = (\max(F_o^2,0) + 2F_c^2)/3$; $a = 0.1067$, $b = 4.3732$. R1 $= \Sigma(|F_o| - |F_c|)/\Sigma(|F_o|)$ and wR2 $= \{\Sigma[w(F_o^2 - F_c^2)^2]/\Sigma[w(F_o^2)^2]\}^{1/2}$ for 2700 reflections with $I > 2\sigma(I)$.

X-ray Crystallography. A red prismatic crystal of **1** with approximate dimensions 0.10 × 0.25 × 0.55 mm was mounted in air. Diffraction measurements were made on a Crystal Logic dual goniometer diffractometer using graphite-monochromated Mo radiation. Important crystal data and parameters for data collection are reported in Table 1. Unit cell dimensions were determined and refined by using the angular settings of 25 automatically centered reflections in the range $11° < 2\theta < 23°$. Intensity data were recorded using a $\theta-2\theta$ scan to $2\theta_{max} = 50°$ with scan speed 1.8°min^{-1} and scan range $2.4 + \alpha_1\alpha_2$ separation. Three standard reflections, monitored every 97 reflections, showed less than 3% intensity fluctuation and no decay. Lorentz and polarization corrections were applied using Crystal Logic software.

The lack of systematically absent reflections results in 16 possible hexagonal space groups, the simplest being $P3$ and $P\bar{3}$. At first we solved the structure in the centrosymmetric $P\bar{3}$ but continued to collect data to cover the $P3$ case too. The refinement in $P\bar{3}$ proved successful, and all our efforts to refine the structure in the non-centrosymmetric $P3$ were not giving better results. The other possible space groups were rejected because they imply symmetry elements through the trinuclear anion, which were not possible. Symmetry equivalent data were averaged with $R_{int} = 0.0436$ to give 3383 independent reflections from a total 6610 collected. The structure was solved by direct methods using SHELXS-86[25] and refined by full-matrix least-squares techniques on F^2 with SHELXL-97[26] using 3383 reflections and refining 265 parameters. All non-H atoms of the trinuclear moiety and the ammonium cation were refined anisotropically while the water molecules of crystallization were refined isotropically with occupation factors free to vary. The central hydroxyl oxygen and the nitrogen of the NH_4^+ sit on a C_3 symmetry axis at $^1/_3$, $^2/_3$, z and $^2/_3$, $^1/_3$, z, respectively. The hydrogens of the orotate ligands were located by difference maps and were refined isotropically while that of the central hydroxyl group was not found, since it should be disordered due to the C_3 axis. The assignment of the central oxygen as hydroxo (and not oxo) is based on the charge balancing of the complex. No hydrogen atoms for the ammonium counterion and the water solvent molecules were included in the refinement. The final values R1 and wR2 for observed data are listed in Table 1; for all reflections used they were 0.0788 and 0.1908,

(22) (a) Bond, A. M.; Clark, R. J. H.; Humphrey, D. G.; Panagiotopoulos, P.; Skelton, B. W.; White, A. H. *J. Chem. Soc., Dalton Trans.* **1998**, 1845. (b) Blake, A. B.; Yavari, A.; Hatfield, W. E.; Sethulekshmi, C. N. *J. Chem. Soc., Dalton Trans.* **1985**, 2509 and references therein. (c) Hendrickson, D. N.; Oh, S. M.; Dong, T.; Kambara, T.; Cohn, M. J.; Moore, M. E. *Comments Inorg. Chem.* **1985**, *4*, 329. (d) Nakamoto, T.; Katada, M.; Kawata, S.; Kitagawa, S.; Kikuchi, K.; Ikemoto, I.; Endo, K.; Sano, H. *Chem. Lett.* **1993**, 1463. (e) Sato, T.; Ambe, F.; Endo, K.; Katada, M.; Maeda, H.; Nakamoto, T.; Sano, H. *J. Am. Chem. Soc.* **1996**, *118*, 3450.

(23) Anson, C. E.; Bourke, J. P.; Cannon, R. D.; Jayasooriya, U. A.; Molinier, M.; Powell, A. K. *Inorg. Chem.* **1997**, *36*, 1265 and references therein.

(24) (a) Poganiuch, P.; Liu, S.; Papaefthymiou, G. C.; Lippard, S. J. *J. Am. Chem. Soc.* **1991**, *113*, 4645. (b) Saalfrank, R. W.; Trummer, S.; Krautscheid, H.; Schünemann, V.; Trautwein, A. X.; Hien, S.; Stadler, C.; Daub, J. *Angew. Chem., Int. Ed. Engl.* **1996**, *35*, 2206.

(25) Sheldrick, G. M. *SHELXS-86: Structure Solving Program*; University of Göttingen: Göttingen, Germany, 1986.

(26) Sheldrick, G. M. *SHELXL-97: Crystal Structure Refinement*; University of Göttingen: Göttingen, Germany, 1997.

respectively. The maximum and minimum residual peaks in the final difference map were 0.865 and −0.403 e/Å^3. The largest shift/esd in the final cycle is 0.007.

Results and Discussion

Synthesis. The coordination chemistry of H_3L with trivalent metals has received rather scant attention, contrary to various mono- and divalent metals for which their orotate complexes are known. To the best of our knowledge, only the cobalt(III) orotate(−2) complex $[Co(OH)(HL)(H_2O)(NH_3)]_n$ has been structurally characterized.[15b] Since we are interested in polynuclear complexes of high-spin metal ions, such as iron(III), in order to investigate their magnetic properties and understand their dynamic phenomena we scheduled the reactions of H_3L with iron(III).

H_3L is insoluble in alcohols, chlorocarbons, CH_3CN, and cold H_2O, being soluble only in hot H_2O. Surprisingly, the potassium and sodium orotate(−1) salts present a very low solubility in H_2O, a fact applied in analytical chemistry.[27] The corresponding ammonium salt shows much greater solubility in H_2O, probably due to efficient ion solvation, but it still presents low solubility in MeOH. Complex **1** was synthesized by addition of concentrated aqueous NH_3 to an equimolar methanolic solution of H_3L. No significant change in solubility was noticed. Upon addition of $FeCl_3 \cdot 6H_2O$ the solution turned orange. As the reaction proceeded, the amount of H_3L was reduced and the color of the solution gradually became red, giving evidence of complex formation. Filtration of the insoluble quantity of H_3L and slow evaporation of the filtrate at room temperature yielded a mixture of red crystals of **1** and an orange material, which has yet to be obtained in a form suitable for X-ray analysis. Fortunately, the orange powder is soluble in MeOH and can be easily removed.

Attempts to synthesize the sodium and potassium salts of compound **1** failed, due to the formation of their insoluble orotic salts. We have also tried to change the reaction solvent, but our attempts did not prove successful, since in CH_3CN as well as in CH_2Cl_2 the immediate formation of an orange-red powder in a mixture with unreacted orotic acid did not permit their separation due to their insolubility in common solvents.

In the IR spectrum, complex **1** exhibits medium-intensity bands at 3430, 3180, 3120, and 3010 cm^{-1}, assignable to $\nu(OH)_{H_2O}$, $\nu(OH)_{OH^-}$, $\nu(NH)_{NH_4^+}$, and $\nu(NH)_{H_2or^-/Hor^{2-}}$. We did not attempt an exact assignment. The broadness and relatively low frequency of these bands are both indicative of strong hydrogen bonding. The spectrum exhibits six bands in the ketone/carboxylate regions (1720−1550 and 1450−1350 cm^{-1}). The two-band pattern at 1402 and 1382 cm^{-1} is assigned[9,17] to the $\nu_s(CO_2)$ mode of the carboxylate groups of H_2L^- and HL^{2-}. The four-band pattern at 1713, 1682, 1636, and 1610 cm^{-1} is assigned[9,17] to the $\nu_{as}(CO_2)$ mode of the carboxylate groups (1682 and 1610 cm^{-1}) and the CO stretching mode (1713 and 1636 cm^{-1}) of the carbonyl groups. The great frequency separation of the ν(CO) bands reflects the presence of both free and coordinated carbonyl groups, in accord with the crystal structure of **1**.

Description of the Structure. An ORTEP plot of the anion of **1** is shown in Figure 1; selected bond distances and angles are listed in Table 2. The central μ_3-hydroxo group lies on a 3-fold axis, and as a consequence the whole molecule presents trigonal symmetry. The three Fe^{III} atoms form an obligatory equilateral triangle of 3.312 Å edge, and the whole $[Fe_3O_{hydroxy}]^{8+}$ core is planar. Each one of the crystallographically equivalent Fe^{III} atoms has a distorted octahedral NO_5 coordination geometry. The NO_5 type of coordination has also been observed in $[Fe_3(\mu_3\text{-}O)(O_2CPh)_6(py)_3]NO_3 \cdot CH_2Cl_2$ (**2**), one of the most recently reported representatives of the "basic carboxylates" family.[22a]

Orotic acid presents two novel types of coordination (**VIII**, **IX**) being in its mono- and dianionic form in the same compound. **1** is the first orotate complex in which the H_2L^- and HL^{2-} ligands coexist. The three H_2L^- are coordinated through their carboxylate oxygens, each carboxylate group being in the familiar bidentate *syn,syn* $\eta^1{:}\eta^1{:}\mu_2$-bridging mode. The whole Fe−O−C−O−Fe moiety is planar. Each of the three HL^{2-} ions bridges two metal ions adopting the mixed chelating/bridging behavior **IX** that is observed for the first time. The carboxylate oxygen O(11) is directed trans to the μ_3-OH group, while N(11) and O(12) lie in the equatorial plane of their corresponding Fe^{III} atoms.

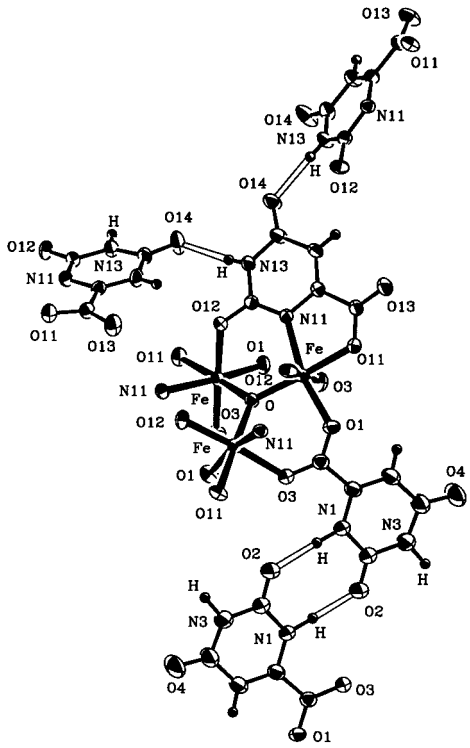

Figure 1. ORTEP plot of the anion of **1** with the atomic labeling (40% thermal probability ellipsoids), also showing the H-bonds (open bonds) forming the 3D network.

Table 2. Selected Bond Distances (Å) and Angles (deg) for **1**·7.75H_2O[a]

	Distances		
Fe−O	1.912(1)	Fe−O(11)	2.026(3)
Fe−O(1)	2.016(3)	Fe−O(12)^{ii}	2.009(3)
Fe−O(3)^{i}	2.060(3)	Fe−N(11)	2.081(4)
	Angles		
O−Fe−O(12)^{ii}	91.7(2)	O(1)−Fe−O(3)^{i}	85.8(1)
O−Fe−O(1)	95.0(1)	O(11)−Fe−O(3)^{i}	89.0(1)
O(12)^{ii}−Fe−O(1)	90.7(1)	O−Fe−N(11)	98.9(1)
O−Fe−O(11)	176.8(1)	O(12)^{ii}−Fe−N(11)	93.0(1)
O(12)^{ii}−Fe−O(11)	88.5(1)	O(1)−Fe−N(11)	165.5(1)
O(1)−Fe−O(11)	88.2(1)	O(11)−Fe−N(11)	77.9(1)
O−Fe−O(3)^{i}	90.9(2)	O(3)^{i}−Fe−N(11)	89.9(1)
O(12)^{ii}−Fe−O(3)^{i}	175.8(1)	Fe−O−Fe^{i}	120.0

[a] Symmetry operations: (i) $1-y, 1+x-y, z$; (ii) $-x+y, 1-x, z$.

(27) (a) Lewis, B. C.; Stephen, W. I. *Anal. Chim. Acta* **1966**, *36*, 234. (b) Pandey, G. S.; Nigam, P. C.; Agarwala, U. *J. Inorg. Nucl. Chem.* **1977**, *39*, 1877.

The three H_2L^- and the three HL^{2-} ligands lie above and below the $Fe_3O_{hydroxy}$ plane. The dihedral angle formed between the $Fe_3O_{hydroxy}$ plane and the plane of the bridging moiety, defined by the carboxylate group and the two Fe^{III} atoms, is 56.7°, while the angle between the planes of $Fe_3O_{hydroxy}$ and the five-membered chelating ring is 31.9°. The orotate rings are planar within experimental error.

Bond distances and angles in the coordination sphere are typical for this class of compounds.[21b−e,g,i,22a,23] The Fe−$O_{hydroxy}$ bond distance is 1.912(1) Å while the Fe−O−Fe angles are exactly 120° due to the trigonal symmetry. The Fe−$O_{carboxylate}$ bond distances are almost equal [Fe−O(1) = 2.016(3) Å, Fe−O(3) = 2.060(3) Å, Fe−O(11) = 2.026(3) Å] but slightly longer than the Fe−$O_{carbonyl}$ [Fe−O(12) = 2.009(3) Å]. The C−O bond distances of the bidentate carboxylate group in H_2L^- are almost identical [C(7)−O(1) = 1.254(6) Å, C(7)−O(3) = 1.252(6) Å] while in the case of HL^{2-} the monodentate coordination of the carboxylate group is reflected in the C−O bond distances [C(17)−O(11) = 1.275(6) Å, C(17)−O(13) = 1.223(6) Å].

As shown in Figure 1, each trinuclear anion is hydrogen bonded to its neighbors, resulting in a 3D structure which becomes much more complicated by the involvement of the ammonium counterion and the water solvate molecules. Each of the H_2L^- ligands is doubly H-bonded to a corresponding ligand of a neighboring trinuclear anion, forming layers along the *bc* plane. These DA = AD type hydrogen bonds involve the pyrimidine carbonyl oxygen and the amide N−H group [N(1)···O(2)′ = 2.877(6) Å, H···O(2)′ = 1.88(8) Å, N(1)−H···O(2)′ = 171(6)°; O(2)′: $-x$, $1-y$, $-z$]. Analogous hydrogen-bond pairs have been observed in the crystal structure of $[Pt_2(PPh_3)_4(HL')]BF_4$ (where HL′ = trianion of 5-aminoorotic acid) resulting in the formation of dimers,[18] and in $[Zn(H_2L')(H_2O)_2]_n$ and $[Zn(H_3L')_2(dmso)_2(H_2O)_2]$ (where H_3L' = 5-aminoorotic acid) participating in the formation of 3D structures.[28] Double hydrogen bonds are found in nature occurring in guanine tetrads (or G quartets)[29] which are stabilized by a central sodium ion. Each of the HL^{2-} ligands is using its noncoordinated carbonyl oxygen and the imido N−H group to form hydrogen bonds with the corresponding ligand of two different anions, forming layers along the *ab* plane [N(13)···O(14)′ = 2.727(6) Å, H···O(14)′ = 1.96(6) Å, N(13)−H···O(14)′ = 176(7)°; O(14)′: x, $1-x+y$, $1-z$]. The pattern of hydrogen bonds involving the orotate ligands is completed by the interference of ammonium ions and water solvents, which interact, with the remaining carbonyl oxygens and NH groups.

Magnetic Behavior. The temperature dependence of the molar magnetic susceptibility of complex **1**, in the form of $\chi_M T$, is shown in Figure 2. The product $\chi_M T$ (4.89 $cm^3\ mol^{-1}$ K at 301 K) decreases steadily with decreasing temperature, reaching the value of 0.85 $cm^3\ mol^{-1}$ K at 3 K. The room-temperature $\chi_M T$ product is appreciably lower than expected for three uncoupled $S = {}^5/_2$ spins (13.13 $cm^3\ mol^{-1}$ K) and clearly reveals the antiferromagnetic behavior of the complex **1** while the low-temperature $\chi_M T$ data does not extrapolate to zero as temperature approaches 0 K.

In order to investigate the magnetic behavior of the trinuclear system, a spin-only Heisenberg−Dirac−van Vleck (HDvV) Hamiltonian formalism was used and a C_{2v} point-group symmetry was assumed for the system.

$$H = -2J_1(\mathbf{S}_1\cdot\mathbf{S}_2 + \mathbf{S}_1\cdot\mathbf{S}_3) - 2J_2(\mathbf{S}_2\cdot\mathbf{S}_3) \qquad (1)$$

The energies of the spin states as functions of the exchange integrals J_1 and J_2 were derived by using the Kambe[30] vector-coupling approach,

$$E(\mathbf{S}_T,\mathbf{S}_{23}) = -J_1\cdot\mathbf{S}_T(\mathbf{S}_T+1) + (J_1-J_2)\cdot\mathbf{S}_{23}(\mathbf{S}_{23}+1) \qquad (2)$$

where $S_{23} = S_2 + S_3$ and $S_T = S_1 + S_{23}$. Although the point-group symmetry of our system is C_{3v}, no satisfactory fitting was obtained by assuming $J_1 = J_2 = J$. This happens because of the topology of the magnetic ions (an ideal equilateral triangle) which leads to nonpreferred spin vector alignment ($J < 0$). Having in mind that the interactions are antiferromagnetic, the energy of the spin states depends on S_{23} and in our case the term J_1/J_2 for some *discrete* values could lead to accidental degeneracy and other interesting phenomena of spin frustration. Figure 3 displays (a) the dependence of the term $\alpha = J_1/J_2$ with some energy levels of the trinuclear system and (b) the case of spin frustration for the value of $\alpha = 0.57$ where the energy levels, in the form of (S_T,S_{23}), ($^3/_2$,1) and ($^1/_2$,2) are accidentally

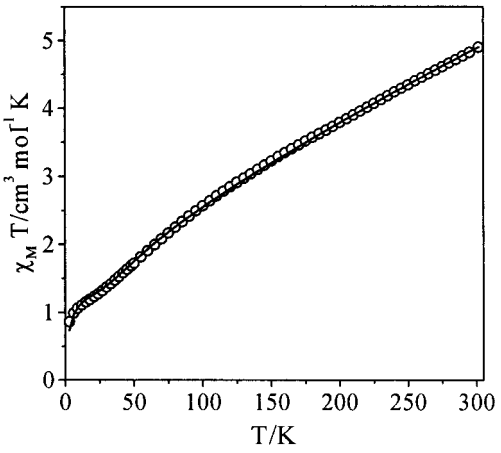

Figure 2. Temperature dependence of the magnetic susceptibility, in the form of $\chi_M T$, in temperature range T = 3−300 K. The solid line represents the fit according to eq 2 with the addition of mean-field corrections.

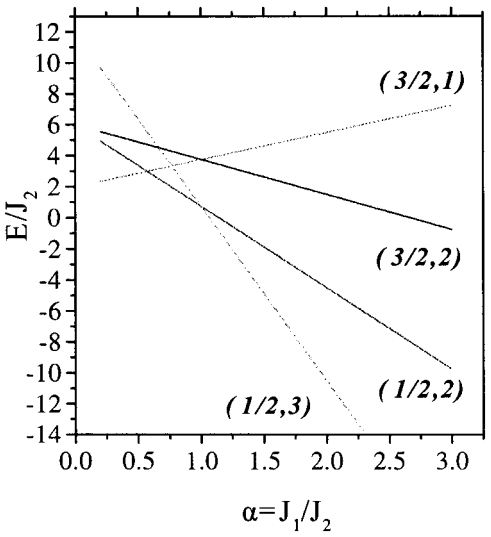

Figure 3. Dependence of some selective energy levels on the parameter $\alpha = J_1/J_2$.

(28) Lalioti, N.; Raptopoulou, C. P.; Terzis, A.; Panagiotopoulos, A.; Perlepes, S. P.; Manessi-Zoupa, E. *J. Chem. Soc., Dalton Trans.* **1998**, 1327.
(29) Laughlan, G.; Murchie, A. I. H.; Norman, D. G.; Moore, M. H.; Moody, P. C. E.; Lilley, D. M. J.; Luisi, B. *Science* **1994**, *265*, 520.
(30) Kambe, K. *J. Phys. Soc. Jpn.* **1950**, *5*, 48.

degenerate. When $\alpha = 1$, the energy of the spin states does not depend on the intermediate spin S_{23} and the ground state is given by two degenerate spin doublets, arising from $S_{23} = 2$ and $S_{23} = 3$. The ground state of the system is (a) $S = {}^3/_2$ for values $0 < \alpha < 0.57$, (b) $S = {}^1/_2$ for values $\alpha > 0.57$, where only the value of the intermediate spin quantum number S_{23} changes for $\alpha > 1$ (Figure 3).

A fit to the data of Figure 2 gives $J_1 = -19.2$ cm^{-1}, $J_2 = -32.3$ cm^{-1} ($\alpha = 0.60$), and $g = 2.0$ fixed ($R = 2.92 \times 10^{-4}$). The energy spectrum reveals that the energy difference between the ground spin doublet and the first excited multiplet, which is characterized by $S_{23} = 1$, $S_T = {}^3/_2$, is 5.2 cm^{-1}. A very important feature of this system is its interconnection with other similar units through extended hydrogen bonds revealing a complex 3D network. In order to investigate the role of the hydrogen bonds in the magnetic behavior of the system, several magnetic models were used to fit the low-temperature behavior of the susceptibility data.

Zero-Field Contributions. Applying the term $D(\mathbf{S}^2_z - 1)$ to the above magnetic model resulted in no net improvement of the quality of the fit. The value of $D = -0.3$ cm^{-1} was obtained but reveals that it does not play an important role in the magnetic behavior of the system in the low-tempetaure range.

Non-Heisenberg Exchange Contributions. An alternative explanation for the magnetic behavior of complex **1** retaining its idealized trigonal symmetry is the presence of non-Heisenberg exchange contributions. By adding antisymmetric exchange (AS) terms[29] to the above magnetic model in a magnetic field H and using perturbative treatment (assuming that the leading contribution to the Hamiltonian, **H**, comes from the Heisenberg exchange terms), we tried to apply them to the ground state of complex **1**, while retaining $J_1 = J_2$. The Hamiltonian form is

$$\mathbf{H} = \mathbf{H}_{\mathrm{HDvV}} + \mathbf{G}[(\mathbf{S}_1 \times \mathbf{S}_2) + (\mathbf{S}_2 \times \mathbf{S}_3) + (\mathbf{S}_3 \times \mathbf{S}_1)] + g\mu_B \mathbf{H}\cdot\mathbf{S}_T \quad (3)$$

where **G** is the antisymmetric exchange vector and we assume $G_x = G_y = 0$, for C_{3v} symmetry. For $S = {}^5/_2$ spins the energy of the four magnetic sublevels of the ground state is given by

$$\mathrm{E(H)} = \pm 0.5[\mathrm{D}^2 + (g\mu_B \mathrm{H})^2 \pm 2g\mu_B \mathrm{HD}\cos\theta\,]^{1/2} \quad (4)$$

where $H = |\mathrm{H}|$, $D = D_z = 9(3)^{1/2}G_z$, and θ is the angle between the field and the z axis.[31] However, no net improvement of the fit resulted, showing that the overall picture of the energy spectrum arising from the C_{3v} Heisenberg magnetic model is incorrect while AS terms do not influence the magnetic behavior of the system.

Mean-Field Corrections. Applying the term $-zJ\langle Sz\rangle\mathbf{Sz}$ to the above magnetic model an important improvement of the fit in the low-temperature range resulted in the following set of fitting parameters: $J_1 = -18$ cm^{-1}, $J_2 = -31.2$ cm^{-1}, and $zJ = -1.0$ cm^{-1}. This theoretical expression is shown as a solid line in Figure 2. It is important to note that the value $\alpha = J_1/J_2$ for this set of parameters is 0.58 and leads to an almost degeneracy of ($^1/_2$,2) and ($^3/_2$,1), the energy difference being 1.2 cm^{-1}. It seems that the role of the hydrogen bonds is important in the frustrated behavior of the system. The energy spectrum according to this model and that of eq 2 is shown in Figure 4.

Further investigating the magnetic behavior of the system, magnetization measurements were taken in the temperature

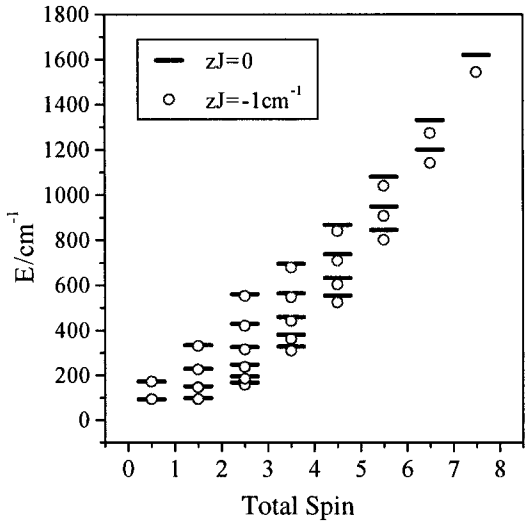

Figure 4. Energy spectrum vs total spin according to the fitting parameters of the two different magnetization models (a) eq 2 and (b) eq 2 and mean-field corrections.

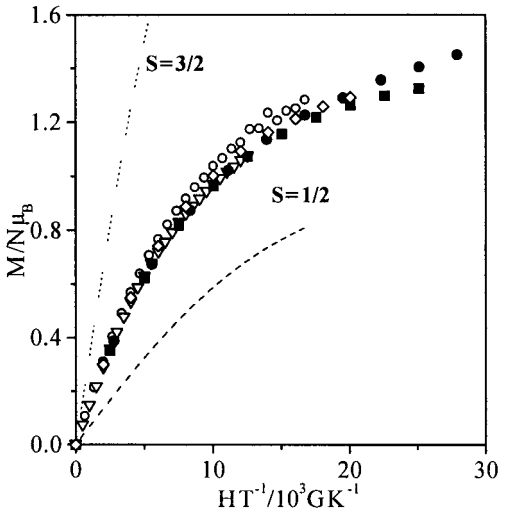

Figure 5. Magnetization measurements in the field range 0−5 T and in various temperatures in the range $T = 1.8$−4 K (●, 1.8 K; ■, 2 K; ◇, 2.5 K; ○, 3 K; ▽, 4 K).

range 1.8−4 K and in the field range 0−5 T and are shown in Figure 5. The two dotted lines in the same figure represent the Brillouin functions for an $S = {}^1/_2$ and $S = {}^3/_2$ system, respectively, and clearly show that the nature of the ground state is intermediate between these two. We used a more general magnetization[32] equation which takes into consideration (a) the first excited state and (b) the energy difference between the ground and the first excited state according to the energy spectrum derived from the susceptibility data. The general thermodynamic relation is

$$\mathrm{M} = \mathrm{N}\sum_{i=1}^{P}\left(\frac{-\delta \mathrm{E}_i}{\delta \mathrm{H}}\right)\exp(-\mathrm{E}_i/kT)/\sum_{i=1}^{P}\exp(-\mathrm{E}_i/kT) \quad (5)$$

The two dotted lines in Figure 6 show the simulations of the theoretical magnetization equation for two different sets of parameters (a) $\Delta E = 5.2$ cm^{-1} ($zJ = 0$) and (b) $\Delta E = 1.2$ cm^{-1}

(31) (a) Gorun, S. M.; Lippard, S. J. *Inorg. Chem.* **1991**, *30*, 1625. (b) Turowski, P. N.; Armstrong, W. H.; Roth, M. E.; Lippard, S. J. *J. Am. Chem. Soc.* **1990**, *112*, 681.

(32) Tangoulis, V.; Diamantopoulou, E.; Bakalbassis, E. G.; Raptopoulou, C. P.; Terzis, A.; Perlepes, S. P. *Mol. Cryst. Liq. Cryst.* **1999**, *335*, 463.

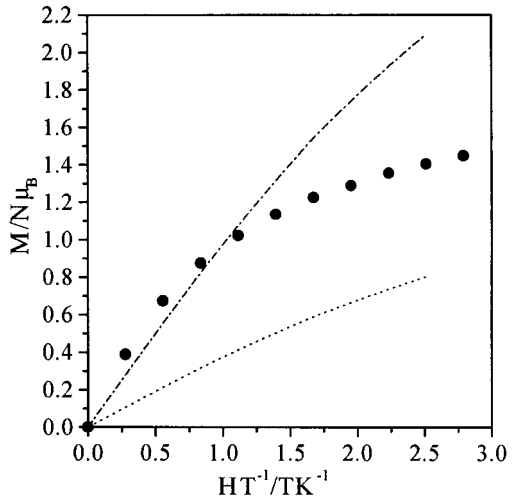

Figure 6. Experimental magnetization measurements at 1.8 K. The two dotted lines represent simulations of the generalized magnetization eq 5 according to the two theoretical models. See text for details.

($zJ = -1$ cm^{-1}). The solid dots represent the magnetization data at $T = 1.8$ K.

Complex **1** is the first complex in the series of "basic carboxylates" where the first excited state is only 1 cm^{-1} higher and phenomena like spin frustration seem to influence its magnetic behavior. The energy gap in those complexes[33] is around 50 cm^{-1} while in the case of an alkoxo cluster,[34] $Fe_3(\mu\text{-}OCH_3)(\mu\text{-}OCH_3)_3(OCH_3)(dbm)_3$, it is 13 cm^{-1}. The structural differences between those complexes and complex **1** are reflected in the magnitude of exchange parameters and the low-temperature dependence of the susceptibility data. Moreover the magnetization measurements reveal the complex character of the ground state where both the singlet and the multiplet are populated.

EPR Studies. Important information about (a) the character of the ground state; (b) the magnitude and the role of the zero-field splitting; and (c) the relative importance of AS- and Heisenberg-exchange contributions can be obtained by X-band EPR spectra. The X-band EPR spectrum of complex **1** at $T = 4$ K is shown in Figure 7. It shows that the $S = {}^3/_2$ ($g = 4.3$) is populated revealing that it is close to the ground state $S = {}^1/_2$ while the central derivative may be assigned to both $S = {}^3/_2$ and $S = {}^1/_2$ states. Efforts to simulate the central derivative with different forms of derivative (Lorentzian, Gaussian, or a mixed type of the previous two) failed, showing the anisotropic character of the spectrum. In the low-field region a peak at $g = 5.7$ retains its magnitude from $T = 4$ K to room temperature, and it may arise from other excited states (probably an $S = {}^5/_2$ one).

Simulation Properties. In order to verify the previous assignment a simulation procedure[35] was carried out based on the following Hamiltonian formalism:

$$H = \mu_B \mathbf{B}\cdot\mathbf{g}\cdot\mathbf{S} + \mathbf{S}\cdot\mathbf{D}\cdot\mathbf{S} \qquad (6)$$

with the following assumptions: (a) the electronic Zeeman interaction is the largest, followed by the zero-field splitting; (b) in order to increase the accuracy of the simulation a second-order perturbation theory was carried out; (c) the only populated state is the $S = {}^3/_2$, and it is well "isolated" from the next nearest excited states; (d) the line widths (W) can vary as a function of the direction of the externally applied magnetic field,

$$W(l_x,l_y,l_z) = \sqrt{w_x^2 l_x^2 + w_y^2 l_y^2 + w_z^2 l_z^2} \qquad (7)$$

where the l_x, l_y, and l_z are the direction cosines of the magnetic field on the electronic Zeeman principal axes and w_x, w_y, and w_z are the line widths along the principal axes; (e) isotropic values for g values.

The simulation spectrum along with the experimental one is shown in Figure 7, and the parameters are $D = 0.2$ cm^{-1}, $E = 0.064$ cm^{-1} ($\lambda = 0.3$), $w_x = w_y = 300$ G, $w_z = 600$ G, $g = 2.0(1)$ while the type of the spectrum is [0.6 Lorentzian + 0.4 Gaussian]. The results confirm our previous assignment of the anisotropic character of the spectrum. Figure 8 displays the λ-dependence of the spectrum by keeping fixed the value of D and changing only the E parameter.

Mössbauer Spectra. Mössbauer spectra were taken in the temperature range 2.1−300 K. The spectra display a doublet in

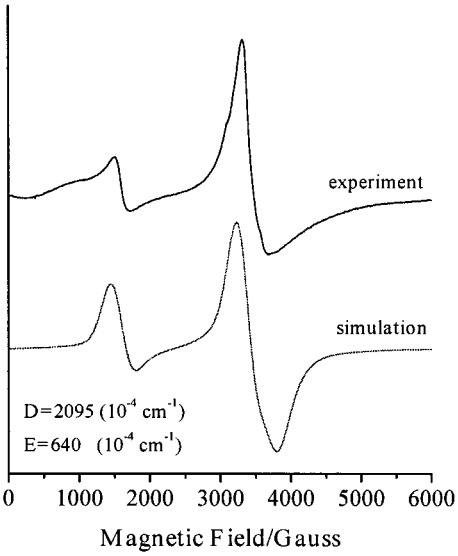

Figure 7. Powder EPR spectum at 4 K and the simulation of it using the Hamiltonian of eq 6.

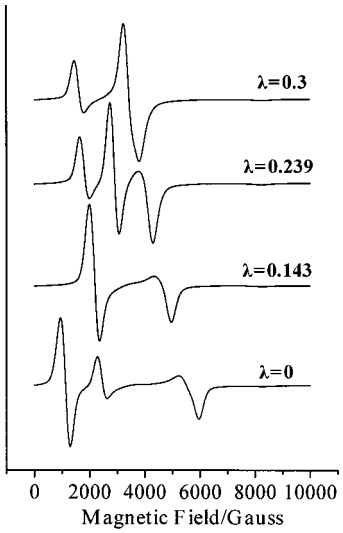

Figure 8. Powder EPR spectra (simulations) for different values of $\lambda = E/D$ (see text).

(33) (a) Rakitin, Yu. V.; Yablokov, Yu. V.; Zelentsov, V. V. *J. Magn. Reson.* **1981**, *43*, 288. (b) Tsukerblat, B. S.; Belinskii, M. I.; Fainzillberg, V. E. *Sov. Sci. Rev., Sect. B* **1987**, *9*, 337 and refererences therein.

(34) Caneschi, A.; Cornia, A.; Fabretti, A. C.; Gatteschi, D.; Malavasi, W. *Inorg. Chem.* **1995**, *34*, 4660.

(35) WIN-EPR *SimFonia* 1.2, Bruker Instruments, 1995.

the whole temperature range with a quadrupole splitting of 1.00 mm/s and isomer shift of 0.39 mm/s (room temperature) with respect to Fe metal. The quadrupole splitting does not show any essential temperature variation. A slight asymmetry of the two peaks is observed at low temperatures ($I_+/I_- = 0.9$) which is reversed above 35 K and becomes $I_+/I_- = 1.1$ at room temperature. The isomer shift is typical of a high-spin trivalent Fe state while the quadrupole splitting reveals an asymmetric charge environment. Low-temperature measurements in the presence of an external field of 6 T display spectra of intermediate spin relaxation character that hinder the evaluation of the spin system.

Conclusions. Orotic acid has proved to be a very interesting ligand in the coordination chemistry of trivalent metal ions, such as iron(III). The product described, $(NH_4)[Fe_3(\mu_3\text{-}OH)(H_2L)_3(HL)_3]\cdot 7.75H_2O$ (**1**), has been structurally characterized, and its magnetic, EPR, and Mössbauer properties have been studied. Compound **1** consists of three Fe^{III} ions arranged at an obligatory equilateral triangle due to the C_3 axis passing through the central hydroxyl oxygen. The orotates present two novel types of coordination with the -1 and -2 forms coexisting in the same compound. It is clear that the nature of orotic acid makes its various anionic forms versatile for use with a variety of metals and for a variety of objectives/advantages, including variable denticity levels, bridging vs terminal modes, high-nuclearity aggregate formation, and the linking of aggregates into polymeric arrays. The central $Fe_3O_{hydroxy}$ moiety is planar with the three monoanionic and the three dianionic orotates arranged above and below this plane. The hydrogen bonds formed between the orotates result in the formation of a 3D structure, while a plethora of H-bonds is also formed between the ligands and the ammonium counterion as well as the solvent molecules. The magnetic behavior of compound **1** is rationalized on the basis of a $2J$ model with the application of mean-field corrections due to the extended hydrogen bonding 3D network and is consistent with the presence of antiferromagnetic interactions between the metal centers as well as between the trimers. Antisymmetric exchange and zero field contributions were taken into account in order to explain the magnetic behavior, but they seem to play a minor role. The EPR measurements are in accordance with the magnetic results showing that the ground state $S = {}^1/_2$ is very close to the first excited $S = {}^3/_2$ which is well populated at 4 K. The compound **1** is a good candidate to investigate the effect of spin frustration in the magnetic behavior of the system.

Acknowledgment. The authors wish to thank Prof. S. P. Perlepes and Dr. A. Terzis for helpful discussions during this research program, Dr. A. Simopoulos for the Mössbauer measurements and useful discussions, and Dr. M. Papadopoulos (Institute of Radioisotopes and Radiodiagnostic Products, NCSR "Demokritos") for all the help provided. We are also grateful to Mr. John Boutaris and the Agricultural Bank of Greece (ATE) for financial support to the Crystallography Laboratory of the Institute of Materials Science of NCSR "Demokritos".

Supporting Information Available: ORTEP plot of the trinuclear compound **1**. This material is available free of charge via the Internet at http://pubs.acs.org.

IC9914084